

Enforcing Mutual Consistency of Hard Regions for Semi-supervised Medical Image Segmentation

Yicheng Wu^{a,*}, Zongyuan Ge^{b,c}, Donghao Zhang^c, Minfeng Xu^d, Lei Zhang^d,
Yong Xia^e, Jianfei Cai^a

^a*Department of Data Science & AI, Faculty of Information Technology,
Monash University, Melbourne, VIC 3800, Australia*

^b*Monash-Airdoc Research, Monash University, Melbourne, VIC 3800, Australia*

^c*Monash Medical AI, Monash eResearch Centre, Melbourne, VIC 3800, Australia*

^d*DAMO Academy, Alibaba Group, Hangzhou, 311121, China*

^e*School of Computer Science and Engineering, Northwestern Polytechnical University,
Xi'an 710072, China*

Abstract

In this paper, we proposed a novel mutual consistency network (MC-Net+) to effectively exploit the unlabeled hard regions for semi-supervised medical image segmentation. The MC-Net+ model is motivated by the observation that deep models trained with limited annotations are prone to output highly uncertain and easily mis-classified predictions in the ambiguous regions (*e.g.* adhesive edges or thin branches) for the image segmentation task. Leveraging these region-level challenging samples can make the semi-supervised segmentation model training more effective. Therefore, our proposed MC-Net+ model consists of two new designs. First, the model contains one shared encoder and multiple slightly different decoders (*i.e.* using different up-sampling strategies). The statistical discrepancy of multiple decoders' outputs is computed to denote the model's uncertainty, which indicates the unlabeled hard regions. Second, a new mutual consistency constraint is enforced between one decoder's probability output and other decoders' soft pseudo labels. In this way, we minimize the model's uncertainty during training and force the model to generate invariant and low-entropy results in such challenging areas of unlabeled data, in order

*Corresponding Author

Email address: Yicheng.Wu@Monash.edu (Yicheng Wu)

to learn a generalized feature representation. We compared the segmentation results of the MC-Net+ with five state-of-the-art semi-supervised approaches on three public medical datasets. Extension experiments with two common semi-supervised settings demonstrate the superior performance of our model over other existing methods, which sets a new state of the art for semi-supervised medical image segmentation.

Keywords: Mutual consistency, soft pseudo label, semi-supervised learning, medical image segmentation

1. Introduction

Medical image segmentation is a fundamental and critical step to construct a computer-aided diagnosis (CAD) system. Based on the accurate segmentation results, the morphological attributes of organs and tissues can be quantitatively analysed to provide useful basis for clinicians to diagnose diseases. At the same time, with an effective segmentation model, the accurate identification of region of interests (ROI) is significant for the early screening and risk assessment of relevant diseases (Masood et al., 2015).

Recent years have witnessed the remarkable progress of deep methods in medical image segmentation. However, they still suffer from limited performance on many medical tasks. Their sub-optimal performance is mainly attributed to the over-fitting caused by the inadequate training data, as most of medical image segmentation datasets are of small scale. This is because acquiring enough densely annotated medical data is extremely expensive. Manually annotating medical images (*e.g.*, volumetric CT or MRI scans) at the pixel/voxel-level not only requires expertise and concentration but also is costly and time-consuming. Therefore, utilizing unlabeled medical data like semi-supervised approaches has become extremely important to improve the training of medical image segmentation models and has attracted increasing research attention.

Existing semi-supervised methods can be roughly divided to two categories. The first approaches are the consistency-based models (Yu et al., 2019; Luo et al.,

2021a,b) according to the smoothness assumption *i.e.* certain perturbations of an input should not produce the obvious deviations of different outputs (Laine and Aila, 2016). The second category consists of several entropy-minimization methods (Lee et al., 2013; Rizve et al., 2021; Pham et al., 2021), which are based on the clustering assumption *i.e.* the cluster of each class should be compact and low entropy. However, most of existing methods do not make full use of the spatial or region-level attributes of results in semi-supervised segmentation tasks. Considering deep models can generate the segmentation results with different pixel/voxel-level uncertainties, we suggested to leverage such uncertainty to effectively exploit the unlabeled data in the region level, aiming to further boost the semi-supervised medical image segmentation.

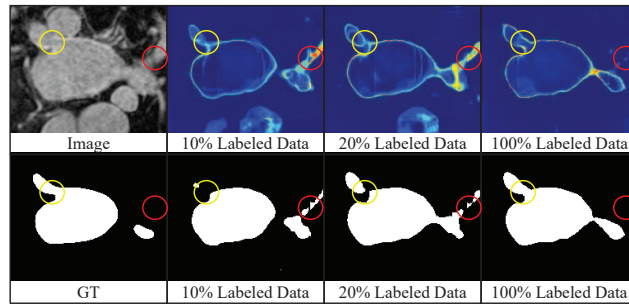


Figure 1: Three exemplar uncertainty maps and the corresponding segmented results of the fully supervised V-Net model, trained with 10%, 20% and all labeled data on the LA dataset.

Our main idea is to regularize the learning of the unlabeled hard regions to facilitate the model training effectively and improve the segmentation performance. Specifically, Fig. 1 shows three uncertainty maps and the segmentation results on the left artium (LA) dataset, which are generated by three fully-supervised V-Net models, respectively trained by 10%, 20% and all labeled data. Each uncertainty map was computed by the Monto-Carlo Dropout (MC-Dropout) method as (Yu et al., 2019). The pixel/voxel-level uncertainty measures the confidences of the deep model’s predictions. Fig. 1 gives two key observations: (1) *The highly uncertain predictions mainly locate on some challenging regions (e.g. thin branch joints, indicated by the yellow and red circles*

in Fig. 1). Meanwhile, the regions without complicated texture and appearance information are more likely to be correctly segmented. In other words, trained with more labeled data, the V-Net only refines the predictions of few challenging areas; (2) *With the increase of labeled data for training, the model is prone to output less ambiguous results.* These observations motivate us to exploit the pixel/voxel-level uncertainty to guide the model to generalize to these hard regions, which also aligns with a concurrent work in (Qiao and Peng, 2021).

Therefore, in this paper, we propose a novel mutual consistency network (MC-Net+) model for semi-supervised medical image segmentation, aiming to pay more attention to unlabeled challenging regions via the model’s uncertainty. First, as Fig. 2 shows, our MC-Net+ model is composed of one shared encoder and multiple slightly different decoders. The statistic discrepancy of multiple decoders’ outputs is used to represent the pixel/voxel-level uncertainty, indicating the unlabeled hard regions. Second, we utilize a sharpening function to convert the probability outputs into the soft pseudo labels. Then, we design a new mutual consistency training scheme, which forces the consistency between one decoder’s probability output and other decoders’ soft pseudo labels. In this way, we minimize the model’s uncertainty during the model training and establish an ‘end-to-end’ way to help model capture more useful features from the challenging regions of unlabeled data.

Overall, our contributions of this paper are three-fold.

- We designed our MC-Net+ model for semi-supervised segmentation, with the key idea that unlabeled hard regions are critical and need to be better exploited in the training process.
- We introduced a novel mutual consistency scheme to effectively leverage the unlabeled challenging regions, which minimizes the model’s uncertainty and enables the model to learn a generalized feature representation.
- Extensive experiments demonstrate that the proposed MC-Net+ model outperforms five recent methods and sets a new state of the art (SOTA) for semi-supervised medical image segmentation.

The preliminary version of this work appeared in MICCAI 2021 (Wu et al., 2021), which encourages the mutual consistency between two slightly different decoders. This paper substantially extends the conference version. The main extensions include: (1) embedding another decoder using a nearest interpolating operation into the original MC-Net model, which further increases the model’s diversity; (2) conducting experiments on the extra Pancreas-CT and ACDC datasets to demonstrate the general effectiveness of our model on other semi-supervised medical image segmentation tasks; (3) implementing five recent approaches in the same environment and reporting the corresponding results for fair comparisons; (4) adopting the original encoder-decoder architecture for testing and achieving the SOTA semi-supervised segmentation performance, without introducing additional computational costs during testing.

2. Related Work

2.1. Semi-supervised Learning

Semi-supervised learning (SSL) is widely studied in various computer vision tasks. For the consistency-based models, various data augmentation methods (Zhang et al., 2017; Xie et al., 2019) can be used to generate the augmented samples. For example, Ouali et al. (2020) enforced several data augmentation operations to the intermediate feature maps and constrained the model to output invariant segmentation maps. Wang et al. (2021) utilized the semantic direction in the feature space to achieve semantic data augmentation and then applied consistency constraints for SSL. Sohn et al. (2020) employed the consistency of training samples under weak and strong perturbations to facilitate the model training. Consistency in the model parameters is also discussed in the mean teacher model via using an exponential moving average (EMA) operation (Tarvainen and Valpola, 2017). At the same time, the adversarial training (Miyato et al., 2018; Mittal et al., 2019) is further used to apply the consistency constraints to enhance the SSL.

Meanwhile, the entropy minimization-based models also can boost the semi-supervised learning. For instance, [Kalluri et al. \(2019\)](#) proposed an entropy module to enable the model to generate low-entropy predictions on the unlabeled dataset. Furthermore, another representative method is known as the pseudo label learning ([Lee et al., 2013](#); [Chen et al., 2021](#)). They often employ a sharpening function or a fixed threshold to convert probability maps into pseudo labels. Then, supervised by pseudo labels, the model can learn to generate low-entropy results. For example, [Rizve et al. \(2021\)](#) unitized the probability and uncertainty thresholds to select the most accurate pseudo labels for SSL. Additionally, [Pham et al. \(2021\)](#) incorporated the meta learning scheme into the pseudo label learning to improve the popular teacher student model.

It is nowadays widely recognized that both the consistency constraints and the pseudo label learning can boost the feature discriminatory power of semi-supervised models. Therefore, in this paper, we employ both techniques in our MC-Net+ model for accurate semi-supervised medical image segmentation.

2.2. Semi-supervised medical image segmentation

Currently, several SOTA semi-supervised methods have been proposed for the medical image segmentation task. For example, [Yu et al. \(2019\)](#) proposed an uncertainty-aware mean-teacher model for semi-supervised left atrium segmentation. [Li et al. \(2020\)](#) further enforced the shape constraints via introducing the signed distance map (SDM) ([Ma et al., 2020](#)) to improve the performance. Meanwhile, [Luo et al. \(2021a\)](#) studied the relation between medical image segmentation and organ shape regression. They also investigated a semi-supervised model to learn multi-scale consistency for the gross target volume (GTV) segmentation ([Luo et al., 2021b](#)). Furthermore, [Xia et al. \(2020\)](#) employed a multi-view co-training strategy to conduct ensemble learning for 3D medical image segmentation. [Xie et al. \(2020\)](#) utilized the attention mechanism to extract the pair-wise relation between labeled and unlabeled data to further relieve the over-fitting caused by limited labeled data.

Although these models have reported encouraging results for medical image

segmentation, they still neglect or underestimate the effects of the unlabeled challenging regions during the model training. In other words, we hypothesize that the performance of semi-supervised image segmentation can be further improved via more effective modeling the challenging regions even without corresponding labels.

2.3. Uncertainty Estimation

Recently, uncertainty analysis attracts much attention in the both fields of machine learning and medical image processing (Abdar et al., 2021; Jungo and Reyes, 2019). We not only expect the model output correct results, but also hope to obtain the confidence of the results. For example, the inherent aleatoric uncertainty is caused by the annotation noises and the epistemic uncertainty accounts for uncertainty of the deep models (Kendall and Gal, 2017). In semi-supervised scenarios, we here only discuss the epistemic uncertainty, which can be reduced by giving more training data.

For instance, Jin et al. (2019) employed the variational U-Net (Esser et al., 2018) to estimate the model’s uncertainty. Furthermore, the epistemic uncertainty can be quantified via the model ensemble strategy (Lakshminarayanan et al., 2016), which computes the statistical discrepancy of several different models’ outputs and the models are trained individually. However, this scheme would introduce more computational costs. To address this, in Bayesian modeling, the MC-Dropout method is proposed to approximate the model’s uncertainty in a flexible way (Gal and Ghahramani, 2016). Specifically, the dropout operation can sample multiple sub-models from the whole model. The statistical discrepancy of sub-models’ outputs can be used to compute the model’s uncertainty. Therefore, there is no need to train multiple models individually.

To further reduce the computational costs, inspired by (Zheng and Yang, 2021), our model pre-defined the sub-models before the model training, which can estimate the model’s epistemic uncertainty in only one forward pass.

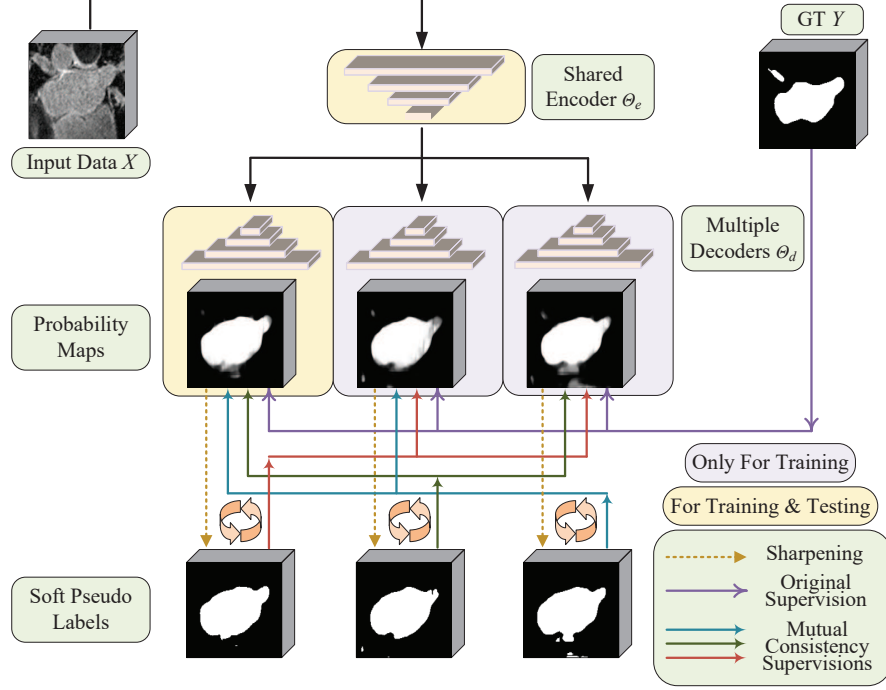


Figure 2: Diagram of our proposed MC-Net+ model, where the mutual consistency constraint is applied between one decoder’s probability output and the other decoders’ soft pseudo labels. Note that, in this paper, there are three slightly decoders in our MC-Net+ model.

3. Method

3.1. Model Architecture

Fig. 2 shows the architecture of our proposed MC-Net+ model. Before introducing our model, we first define the semi-supervised segmentation problem with a set of notations. We use $x \in \mathbb{R}^I$ to denote an input vector and $p(x|\theta) \in \mathbb{R}^I$ is the probability map of an input x , where I is the input dimension and θ denotes the deep model. Let $y \in \mathbb{R}^I$ denotes few annotations. The labeled dataset and unlabeled dataset are denoted as $\mathbb{D}_L = \{x_l^i, y_l^i | i = 1, \dots, N_l\}$ and $\mathbb{D}_U = \{x_u^i | i = 1, \dots, N_u\}$. We use both datasets \mathbb{D}_L and \mathbb{D}_U to train our semi-supervised model in this paper. Hence, the uncertainty estimation process is

defined as the following:

$$\begin{aligned}\theta_{sub} &= Sampling(\theta) \\ \mu_x &= D[p(x|\theta_{sub}^1), \dots, p(x|\theta_{sub}^n)]\end{aligned}\tag{1}$$

where D computes the statistical discrepancy of n probability maps. $\mu_x \in \mathbb{R}^I$ is the pixel/voxel-level uncertainty of x . In MC-Dropout, the dropout operation samples n sub-models from the whole model θ .

To address the issue that MC-Dropout requires a lot of forward passes, we design our model by one encoder and n slightly different decoders, based on the popular encoder-decoder backbone (Milletari et al., 2016; Ronneberger et al., 2015). With a shared encoder θ_e , we pre-define n sub-models before the uncertainty estimation. The uncertainty μ_x can be approximated via our proposed MC-Net+ model formulated as:

$$\begin{aligned}\theta_{sub}^i &= \theta_e \boxplus \theta_d^i, \quad i \in 1, \dots, n \\ \mu_x &= D[p(x|\theta_{sub}^1), \dots, p(x|\theta_{sub}^n)]\end{aligned}\tag{2}$$

where the symbol \boxplus means that the sub-model θ_{sub}^i is composed of one encoder θ_e and one decoder θ_d^i . Thus, each sub-model θ_{sub} is the standard encoder-decoder architecture like V-Net or U-Net. Since the number n of sub-models is scalable, to achieve a nice trade-off between the effectiveness and efficiency, the n is set as 3 in this paper (see Fig. 2).

Specifically, we employ the transposed convolutional layer, the linear interpolation layer and the nearest interpolation layer to construct three slightly different sub-models θ_{sub}^1 , θ_{sub}^2 and θ_{sub}^3 . In this way, we increase the intra-model diversity. Additionally, there are four skip connections in our model, which transfer deep features from encoder to decoder and the decoders do not share parameters. Then, we utilize a convolutional layer to convert the high-dimension features into 2-dimension features. Finally, a SoftMax activation function is used to generate the probability outputs $p^*(x|\theta)$.

3.2. Training via Mutual Consistency

Based on such model design, the divergence of multiple models’ outputs is used to represent the model’s uncertainty and indicates the challenging regions. Then, recalled that both the consistency constraints and the pseudo label learning can help model capture useful features from unlabeled data, we design a novel mutual consistency strategy using two aforementioned constraints to effectively learn the unlabeled challenging regions without labels. Specifically, using a sharpening function (Xie et al., 2019), we first convert an output probability map $p(x|\theta_{sub})$ into a soft pseudo label $p^*(x|\theta_{sub})$ defined as:

$$p^*(x|\theta_{sub}) = \frac{p(x|\theta_{sub})^{1/T}}{p(x|\theta_{sub})^{1/T} + (1 - p(x|\theta_{sub}))^{1/T}} \quad (3)$$

where T is a hyper-parameter to control the temperature of sharpening. Appropriate T not only can enforce the entropy minimization to regularize our model, but also would not introduce additional noises to confuse model.

Afterwards, we perform the mutual learning (Zhang et al., 2018) between one decoder’s probability output and other decoders’ soft pseudo labels. In this way, we minimize such uncertainty to guide the model training rather than directly extract the highly uncertain regions from unlabeled data. The advantages of this can be concluded as: (1) the consistency constraints are enforced via encouraging the invariant outputs of all sub-models; (2) under the supervision of soft pseudo labels, the model is learned to generate low-entropy results as entropy minimization constraints; (3) the MC-Net+ model can be trained in an ‘end-to-end’ manner without multiple forward passes.

Therefore, with the supervision of few annotations y_l , we employ the weighted sum of a supervised loss and a mutual consistency loss to train our proposed MC-Net+ model as the following:

$$L_{mc} = \sum_{i,j=1 \text{ \& } i \neq j}^3 D[p(x|\theta_{sub}^i), p^*(x|\theta_{sub}^j)] \quad (4)$$

$$Loss = L_{seg}(p(x_l|\theta_{sub}^i), y_l) + \lambda \times L_{mc} \quad (5)$$

where L_{seg} is the common Dice loss for the segmentation task. D is adopt as the Mean Squared Error (MSE) loss and receives paired data *i.e.* $p(x|\theta_{sub}^i)$ and $p^*(x|\theta_{sub}^j)$. λ is a hyper-parameter to balance the supervised loss L_{seg} and the mutual consistency loss L_{mc} , which is applied on both \mathbb{D}_L and \mathbb{D}_U .

4. Experiments

4.1. Datasets

We evaluated the proposed MC-Net+ model on the LA, Pancreas-CT and ACDC datasets. The LA dataset (Xiong et al., 2021), the bench-marking dataset for the 2018 Atrial Segmentation Challenge¹, contains 100 gadolinium-enhanced MR imaging scans for training, with an isotropic resolution of $0.625 \times 0.625 \times 0.625$ mm. Since the testing set on LA does not include corresponding annotations, followed by existing models (Yu et al., 2019; Li et al., 2020; Luo et al., 2021a), we applied a fixed split² of 80 samples for training and 20 samples for validation. Then, we report the performance of our model and other methods on the same validation set for fair comparisons.

The Pancreas-CT dataset (Clark et al., 2013) contains 82 3D abdominal contrast enhanced CT scans, which are collected from 53 male and 27 female subjects at the National Institutes of Health Clinical Center³. These slices are collected on Philips and Siemens MDCT scanners and have a fixed resolution of 512×512 with varying thickness from 1.5 to 2.5 mm. The data split is fixed in this paper as the DTC model (Luo et al., 2021a). We employed 62 samples for training and report the performance on the rest 20 samples. We then clipped the voxel values to the range of $[-125, 275]$ hounsfield units (HU) as (Zhou et al., 2019) and further re-sampled the data into an isotropic resolution of $1.0 \times 1.0 \times 1.0$ mm.

¹<http://atriaseg2018.cardiacatlas.org>

²<https://github.com/yulequan/UA-MT/tree/master/data>

³<https://wiki.cancerimagingarchive.net/display/Public/Pancreas-CT>

The ACDC (Automated Cardiac Diagnosis Challenge) dataset was collected from real clinical exams acquired at the University Hospital of Dijon⁴ (Bernard et al., 2018). The ACDC dataset contains cardiac MR imaging samples (multi-slice 2-D cine MRI) from 100 patients for training and 50 patients for testing. Also, following (Luo, 2020), we only selected the original training set in our experiments with a fixed data split⁵ in the patient level, where the new training, validation and testing sets respectively contain 70, 10 and 20 patients’ data. Unlike the task is 3D binary segmentation on the LA and Pancreas-CT datasets, we extend our model to the 2D multi-class segmentation task on the ACDC dataset. The 2D MC-Net+ model is designed to segment four classes including the background, myocardium, left and right ventricles from the MR scans.

4.2. Implementing Details

3D Segmentation: Following (Yu et al., 2019; Li et al., 2020; Luo et al., 2021a), we cropped the 3D samples according to the ground truth, with enlarged margins *i.e.* $[10 \sim 20, 10 \sim 20, 5 \sim 10]$ or $[25, 25, 25]$ voxels on LA or Pancreas-CT, respectively. Then, these scans were normalized as zero mean and unit variance. For training, we randomly extracted 3D patches of size $112 \times 112 \times 80$ on LA or $96 \times 96 \times 96$ on Pancreas-CT.

Afterwards, we applied the 2D rotation and flip operations to the LA dataset for data augmentation. Then, on both datasets, the batch size was set as 4 and each batch contained two labeled patches and two unlabeled patches. The temperature constant T was set as 0.1 on LA and 0.5 on Pancreas. The weight λ was set as a time-dependent Gaussian warming-up function as (Laine and Aila, 2016), which can reduce the impact of inaccurate mutual consistency loss in the early training stage. The 3D backbone was V-Net, which uses the tri-linear interpolation layer to enlarge the feature maps. We trained the 3D MC-Net+ model for 15k iterations. For testing, we employed a sliding window of size

⁴<https://www.creatis.insa-lyon.fr/Challenge/acdc/databases.html>

⁵<https://github.com/HiLab-git/SSL4MIS/tree/master/data/ACDC>

$112 \times 112 \times 80$ or $96 \times 96 \times 96$ with a fixed stride $18 \times 18 \times 4$ or $16 \times 16 \times 16$ to extract patches on the LA or Pancreas-CT dataset, respectively. Then, we recomposed the patch-based predictions as final entire results.

2D Segmentation: On the ACDC dataset, we also normalized the samples as zero mean and unit variance. The random rotation and flip operations were applied as data augmentation. The 2D patches of size 256×256 were randomly extracted and the batch size was set as 24. Each batch included 12 labeled data and 12 unlabeled samples. The temperature T was 0.1. In the testing time, we resized the scans to 256×256 as input and then enlarged it to the original size as final results. Our 2D MC-Net+ model used the U-Net model as the backbone, which utilizes the bi-linear interpolation to expand the feature maps. The 2D model was trained via 30k iterations. All settings on the ACDC dataset were followed the public benchmark (Luo, 2020) for fair comparisons.

On all datasets, we adopt the SGD optimizer with a learning rate 10^{-2} and a weight decay factor 10^{-4} for training. Note that, we performed two typical semi-supervised experimental settings *i.e.* training with 10% or 20% labeled data and the rest unlabeled data as (Yu et al., 2019; Li et al., 2020; Luo et al., 2021a). During testing, we only employed the original encoder-decoder architecture *i.e.* the sub-model θ_{sub}^l . In this paper, we re-implemented all compared methods and conducted the experiments in the identical environment (Hardware: Intel(R) Xeon(R) Gold 6150 CPU@2.70GHz, NVIDIA Tesla V100 GPU; Software: PyTorch 1.8.0, CUDA 11.2 and Python 3.8.10; Random Seed: 1337). Following (Yu et al., 2019; Li et al., 2020; Luo et al., 2021a), we adopt four metrics including Dice, Jaccard, the average surface distance (ASD) and the 95% Hausdorff Distance (95HD) for the quantitative evaluation.

5. Results

Performance on LA: Fig. 3 gives several segmentation results from two samples, in 2D and 3D views, obtained by five recent models and our method on the LA dataset from left to right. It can be seen that the MC-Net+ model

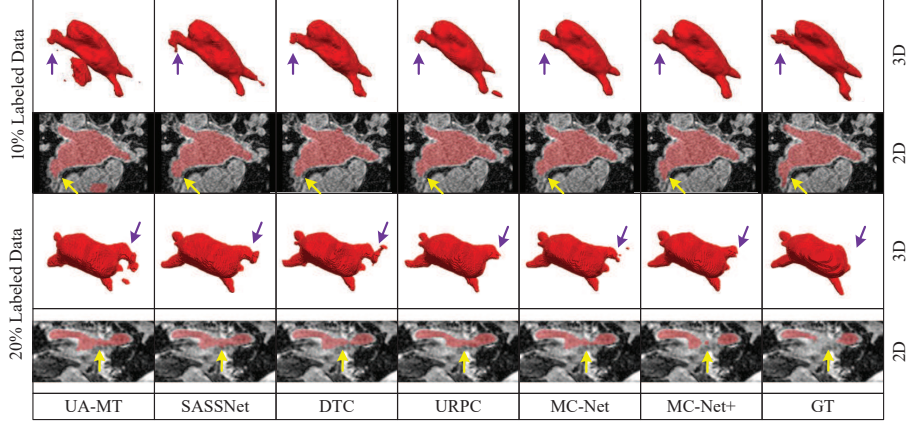


Figure 3: From left to right, there are several exemplar results in 2D and 3D views obtained by the UA-MT (Yu et al., 2019), SASSNet (Li et al., 2020), DTC (Luo et al., 2021a), URPC (Luo et al., 2021a), MC-Net (Wu et al., 2021), our MC-Net+ model, and the corresponding ground truth on the LA dataset.

Table 1: Comparisons with five state-of-the-art methods on the LA dataset.

Method	# Scans used		Metrics				Complexity	
	Labeled	Unlabeled	Dice(%) \uparrow	Jaccard(%) \uparrow	95HD(voxel) \downarrow	ASD(voxel) \downarrow	Para.(M)	MACs(G)
V-Net	8(10%)	0	78.57	66.96	21.20	6.07	9.44	47.02
V-Net	16(20%)	0	86.96	77.31	11.85	3.22	9.44	47.02
V-Net	80(All)	0	91.62	84.60	5.40	1.64	9.44	47.02
UA-MT (Yu et al., 2019) (MICCAI)	8 (10%)	72 (90%)	86.28	76.11	18.71	4.63	9.44	47.02
SASSNet (Li et al., 2020) (MICCAI)			85.22	75.09	11.18	2.89	9.44	47.05
DTC (Luo et al., 2021a) (AAAI)			87.51	78.17	8.23	2.36	9.44	47.05
URPC (Luo et al., 2021b) (MICCAI)			85.01	74.36	15.37	3.96	5.88	69.43
MC-Net (Wu et al., 2021) (MICCAI)			87.50	77.98	11.28	2.30	12.35	95.15
MC-Net+ (Ours)			88.96	80.22	8.02	1.83	9.44	47.02
UA-MT (Yu et al., 2019) (MICCAI)	16 (20%)	64 (80%)	88.74	79.94	8.39	2.32	9.44	47.02
SASSNet (Li et al., 2020) (MICCAI)			89.16	80.60	8.95	2.26	9.44	47.05
DTC (Luo et al., 2021a) (AAAI)			89.52	81.22	7.07	1.96	9.44	47.05
URPC (Luo et al., 2021b) (MICCAI)			88.74	79.93	12.73	3.66	5.88	69.43
MC-Net (Wu et al., 2021) (MICCAI)			90.12	82.12	8.07	1.99	12.35	95.15
MC-Net+ (Ours)			91.07	83.67	5.84	1.67	9.44	47.02

generates more complete left atrium than other SOTA methods. Note that, we do not use any morphological operations to refine the segmented results *e.g.* selecting the largest connected component as the post-processing module (Li et al., 2020). Our model naturally eliminates most of isolated regions and preserves more fine details (indicated by purple and yellow arrows in Fig. 3) for

the semi-supervised left atrium segmentation.

Table 1 shows the quantitative results on the LA dataset. It also gives the results of fully supervised V-Net model with 10%, 20% and all labeled data as the reference. By effectively leveraging the unlabeled data, our proposed MC-Net+ achieves impressive performance gains from 55% to 70% of Dice with only 10% labeled training data. Meanwhile, the model with only 20% labeled training data obtains comparable results, *e.g.* 91.07% vs. 91.62% of Dice, comparing with the upper bound (V-Net with 100% labeled training data). At the same time, as depicted in Table 1, our MC-Net+ model significantly outperforms the other methods in two semi-supervised settings and does not introduce more inference costs compared to the V-Net backbone.

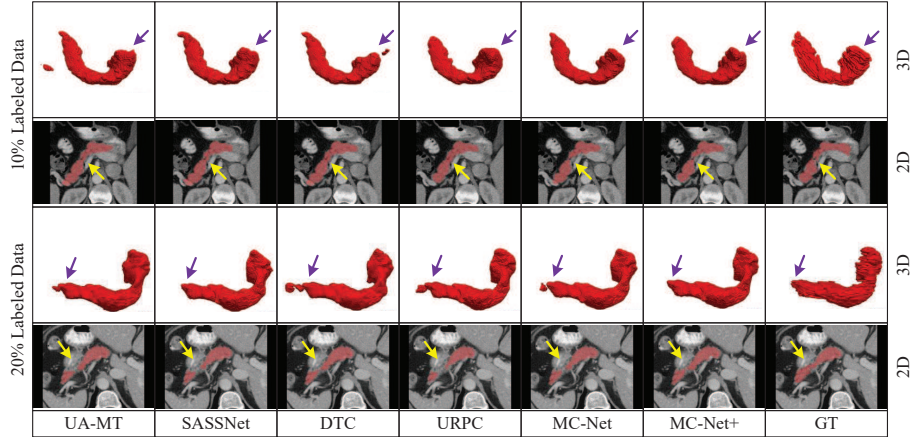


Figure 4: From left to right, there are several exemplar results in 2D and 3D views obtained by the UA-MT (Yu et al., 2019), SASSNet (Li et al., 2020), DTC (Luo et al., 2021a), URPC (Luo et al., 2021a), MC-Net (Wu et al., 2021), our MC-Net+ model, and the corresponding ground truth on the Pancreas-CT dataset.

Performance on PA: Fig. 4 and Table 2 show the corresponding results of our model and five semi-supervised methods on the Pancreas-CT dataset. Except for the multi-scale consistency method (Luo et al., 2021b), our proposed MC-Net+ model achieved the highest Dice and Jaccard than other methods for semi-supervised pancreas segmentation. Actually, the pancreas segmentation is

Table 2: Comparisons with five state-of-the-art methods on the Pancreas-CT dataset. Except the multi-scale model (Luo et al., 2021b), our proposed MC-Net+ model achieves the highest Dice and Jaccard for the semi-supervised pancreas segmentation.

Method	# Scans used		Metrics				Complexity	
	Labeled	Unlabeled	Dice(%) \uparrow	Jaccard(%) \uparrow	95HD(voxel) \downarrow	ASD(voxel) \downarrow	Para.(M)	MACs(G)
V-Net	6 (10%)	0	54.94	40.87	47.48	17.43	9.44	41.45
V-Net	12 (20%)	0	71.52	57.68	18.12	5.41	9.44	41.45
V-Net	62 (All)	0	82.60	70.81	5.61	1.33	9.44	41.45
UA-MT (Yu et al., 2019) (MICCAI)	6 (10%)	56 (90%)	66.44	52.02	17.04	3.03	9.44	41.45
SASSNet (Li et al., 2020) (MICCAI)			68.97	54.29	18.83	1.96	9.44	41.48
DTC (Luo et al., 2021a) (AAAI)			66.58	51.79	15.46	4.16	9.44	41.48
URPC (Luo et al., 2021b) (MICCAI)			73.53	59.44	22.57	7.85	5.88	61.21
MC-Net (Wu et al., 2021) (MICCAI)			69.07	54.36	14.53	2.28	12.35	83.88
MC-Net+ (Ours)			70.00	55.66	16.03	3.87	9.44	41.45
UA-MT (Yu et al., 2019) (MICCAI)	12 (20%)	50 (80%)	76.10	62.62	10.84	2.43	9.44	41.45
SASSNet (Li et al., 2020) (MICCAI)			76.39	63.17	11.06	1.42	9.44	41.48
DTC (Luo et al., 2021a) (AAAI)			76.27	62.82	8.70	2.20	9.44	41.48
URPC (Luo et al., 2021b) (MICCAI)			80.02	67.30	8.51	1.98	5.88	61.21
MC-Net (Wu et al., 2021) (MICCAI)			78.17	65.22	6.90	1.55	12.35	83.88
MC-Net+ (Ours)			79.37	66.83	8.52	1.72	9.44	41.45

a relatively difficult task and may require more multi-scale information. Our model is designed in one scale and should be easily incorporated with other multi-scale methods to further improve the segmentation performance. Note that, we do not enforce any shape-related constrains to train our model and only use the popular Dice loss for the model training. Our model obtains comparable performance in terms of the surface-based metrics. Similar with the results of left atrium, our model does not rely on any post-processing modules and can accurately segment the challenging areas, pointed by the purple and yellow arrows in Fig. 4, on Pancreas-CT.

Performance on ACDC: We further evaluated our model for the 2D multi-class segmentation task on the ACDC dataset. The reported results in Table 3 are the average performance of four classes. It also indicates that: (1) comparing with other methods, our model obtained the highest Dice, Jaccard and comparable surface-related performance in each semi-supervised setting; (2) via exploiting the unlabeled data effectively, on the ACDC dataset, our model almost produced the an average Dice gain of 10% or 3% than the fully-supervised U-Net model trained with 10% or 20% labeled data.

Table 3: Comparisons with five state-of-the-art methods on the ACDC dataset.

Method	# Scans used		Metrics				Complexity	
	Labeled	Unlabeled	Dice(%) \uparrow	Jaccard(%) \uparrow	95HD(voxel) \downarrow	ASD(voxel) \downarrow	Para.(M)	MACs(G)
U-Net	7 (10%)	0	77.34	66.20	9.18	2.45	1.81	2.99
U-Net	14 (20%)	0	85.15	75.48	6.20	2.12	1.81	2.99
U-Net	70 (All)	0	91.65	84.93	1.89	0.56	1.81	2.99
UA-MT (Yu et al., 2019) (MICCAI)	7 (10%)	63 (90%)	81.58	70.48	12.35	3.62	1.81	2.99
SASSNet (Li et al., 2020) (MICCAI)			84.14	74.09	5.03	1.40	1.81	3.02
DTC (Luo et al., 2021a) (AAAI)			82.71	72.14	11.31	2.99	1.81	3.02
URPC (Luo et al., 2021b) (MICCAI)			81.77	70.85	5.04	1.41	1.83	3.02
MC-Net (Wu et al., 2021) (MICCAI)			86.34	76.82	7.08	2.08	2.58	5.39
MC-Net+ (Ours)			87.26	78.30	6.79	1.94	1.81	2.99
UA-MT (Yu et al., 2019) (MICCAI)	14 (20%)	56 (80%)	85.87	76.78	5.06	1.54	1.81	2.99
SASSNet (Li et al., 2020) (MICCAI)			87.04	78.13	7.84	2.15	1.81	3.02
DTC (Luo et al., 2021a) (AAAI)			86.28	77.03	6.14	2.11	1.81	3.02
URPC (Luo et al., 2021b) (MICCAI)			85.07	75.61	6.26	1.77	1.83	3.02
MC-Net (Wu et al., 2021) (MICCAI)			87.83	79.14	4.94	1.52	2.58	5.39
MC-Net+ (Ours)			88.43	80.05	5.20	1.51	1.81	2.99

Therefore, according to the results on three datasets, the MC-Net+ model is a general semi-supervised model for medical image segmentation, which does not rely on specific backbones and can be applied for various medical tasks in either 2D or 3D segmentation. It is obvious that adding another decoder to increase the model’s diversity leads to improved semi-supervised segmentation performance on all datasets (*i.e.* MC-Net+ model vs. MC-Net model (Wu et al., 2021)). Meanwhile, we also observe three interesting attributes of our proposed model: (1) the model can generate better results with less isolated regions; (2) our MC-Net+ is efficient to segment some challenging regions *e.g.* thin branch joints in Fig. 3; (3) for testing, the MC-Net+ model does not introduce more costs. Such ability is essential for further realistic clinical analysis and should be significant to construct an automatic CAD system to diagnose relevant diseases.

6. Discussions

6.1. Ablation Study

The ablation studies (see Table 4) were conducted to show the effectiveness of each design on the LA dataset. It reveals that, in both semi-supervised settings, (1) using multiple slightly different decoders results in an average Dice gain of 1.35% and 0.25%; (2) encouraging the mutual consistency for the model

Table 4: Ablation studies of our proposed MC-Net+ model on the LA dataset.

Method	Output	# Scans used		Metrics			
		Labeled	Unlabeled	Dice(%) \uparrow	Jaccard(%) \uparrow	95HD(voxel) \downarrow	ASD(voxel) \downarrow
V MC-Net+	$\theta_e + \theta_d^{1*}$	8 (10%)	72 (90%)	87.53	78.05	10.73	3.06
	$\theta_e + \theta_d^{2*}$			87.54	78.05	11.14	3.32
	$\theta_e + \theta_d^{3*}$			87.61	78.16	11.98	3.34
	Mean			87.68	78.28	10.44	3.10
MC-Net+ w/ PC	$\theta_e + \theta_d^1$	8 (10%)	72 (90%)	88.65	79.77	9.24	2.20
	$\theta_e + \theta_d^2$			88.79	80.03	8.47	2.04
	$\theta_e + \theta_d^3$			88.96	80.29	8.32	2.05
	Mean			88.84	80.09	8.55	2.05
MC-Net+ w/ PLC	$\theta_e + \theta_d^1$	8 (10%)	72 (90%)	88.70	79.85	8.08	2.03
	$\theta_e + \theta_d^2$			88.78	80.01	7.81	1.91
	$\theta_e + \theta_d^3$			88.55	79.64	8.17	2.00
	Mean			88.71	79.88	7.93	1.93
MC-Net+	$\theta_e + \theta_d^1$	8 (10%)	72 (90%)	88.96	80.25	7.93	1.86
	$\theta_e + \theta_d^2$			88.89	80.15	8.20	1.83
	$\theta_e + \theta_d^3$			88.96	80.26	7.96	1.83
	Mean			88.94	80.22	8.02	1.83
V MC-Net+	$\theta_e + \theta_d^{1*}$	16 (20%)	64 (80%)	90.84	83.32	5.89	1.85
	$\theta_e + \theta_d^{2*}$			90.83	83.30	5.78	1.79
	$\theta_e + \theta_d^{3*}$			90.80	83.26	6.09	1.92
	Mean			90.84	83.32	5.85	1.81
MC-Net+ w/ PC	$\theta_e + \theta_d^1$	16 (20%)	64 (80%)	90.77	83.20	8.27	2.50
	$\theta_e + \theta_d^2$			90.66	83.06	8.39	2.50
	$\theta_e + \theta_d^3$			90.76	83.20	8.17	2.44
	Mean			90.78	83.23	8.22	2.45
MC-Net+ w/ PLC	$\theta_e + \theta_d^1$	16 (20%)	64 (80%)	90.63	83.03	5.99	1.61
	$\theta_e + \theta_d^2$			90.94	83.53	5.86	1.53
	$\theta_e + \theta_d^3$			90.95	83.52	5.85	1.54
	Mean			90.85	83.38	5.92	1.57
MC-Net+	$\theta_e + \theta_d^1$	16 (20%)	64 (80%)	91.07	83.67	5.84	1.67
	$\theta_e + \theta_d^2$			91.07	83.67	5.96	1.58
	$\theta_e + \theta_d^3$			91.08	83.69	5.92	1.58
	Mean			91.08	83.70	5.90	1.60

* Vanilla MC-Net+ model (labeled as V MC-Net+) contains one decoder and three identical decoders (labeled as θ_d^{1*} , θ_d^{2*} and θ_d^{3*} , *i.e.* using the transposed convolution layer).

training is better than applying consistency constraints of the probability outputs or the soft pseudo labels, labeled as PC and PLC; (3) there is no significant

differences between different sub-model’s outputs. Therefore, we only use the original backbone as the testing model in the experiments and thus do not introduce more inference costs.

6.2. Performances with Different Consistency Losses

Table 5: Discussion of different consistency losses to train our model on the LA dataset

Method	Output	# Scans used		Metrics			
		Labeled	Unlabeled	Dice(%) \uparrow	Jaccard(%) \uparrow	95HD(voxel) \downarrow	ASD(voxel) \downarrow
MC-Net+ w/ KL	$\theta_e + \theta_d^1$	8 (10%)	72 (90%)	87.86	78.86	9.65	2.27
	$\theta_e + \theta_d^2$			88.04	79.06	9.42	2.31
	$\theta_e + \theta_d^3$			88.19	79.26	9.30	2.41
	Mean			88.04	79.08	9.40	2.32
MC-Net+ w/ MSE	$\theta_e + \theta_d^1$	16 (20%)	64 (80%)	88.96	80.25	7.93	1.86
	$\theta_e + \theta_d^2$			88.89	80.15	8.20	1.83
	$\theta_e + \theta_d^3$			88.96	80.26	7.96	1.83
	Mean			88.94	80.22	8.02	1.83
MC-Net+ w/ KL	$\theta_e + \theta_d^1$	8 (10%)	72 (90%)	90.93	83.45	6.04	1.63
	$\theta_e + \theta_d^2$			90.98	83.53	6.07	1.58
	$\theta_e + \theta_d^3$			90.96	83.50	6.07	1.58
	Mean			90.96	83.50	6.08	1.60
MC-Net+ w/ MSE	$\theta_e + \theta_d^1$	16 (20%)	64 (80%)	91.07	83.67	5.84	1.67
	$\theta_e + \theta_d^2$			91.07	83.67	5.96	1.58
	$\theta_e + \theta_d^3$			91.08	83.69	5.92	1.58
	Mean			91.08	83.70	5.90	1.60

We further discuss the training effects of different losses to enforce the mutual consistency on the LA dataset. Recalled that D measures the divergence of multiple probability maps, we finally adopt the MSE loss as the distance in this paper. In Table 5, we also give the results of our MC-Net+ model using the Kullback-Leibler (KL) divergence as D for the model training. We can see that the KL loss also can improve the segmentation performance in each semi-supervised setting. Nevertheless, the simple MSE loss is better and sufficient to demonstrate the effectiveness of our model. In other words, our impressive performance gains do not require specific loss function and are led via our designed novel mutual consistency strategy, which effectively modelling the unlabeled hard regions.

7. Conclusion

In this paper, we present a novel MC-Net+ model for semi-supervised medical image segmentation. Effectively leveraging the unlabeled challenging regions plays an important role in the semi-supervised segmentation. Therefore, the architecture design containing three decoders is used to indicate highly uncertain areas and the mutual consistency between the probability outputs and soft pseudo labels establishes an ‘end-to-end’ way to capture more effective features from such hard regions. Extension experiments have demonstrated our model achieved superior performance over five existing models on three medical datasets and the proposed MC-Net+ model sets new state of the art for the semi-supervised medical image segmentation task.

8. Acknowledgments

This work was supported by the Monash FIT Start-up Grant. We also appreciate the efforts devoted to collect and share the datasets (Xiong et al., 2021; Clark et al., 2013; Bernard et al., 2018) and several public benchmarks (Yu et al., 2019; Li et al., 2020; Luo et al., 2021a,b; Luo, 2020).

References

- Abdar, M., Pourpanah, F., Hussain, S., Rezazadegan, D., Liu, L., Ghavamzadeh, M., Fieguth, P., Cao, X., Khosravi, A., Acharya, U.R., et al., 2021. A review of uncertainty quantification in deep learning: Techniques, applications and challenges. *Information Fusion* .
- Bernard, O., Lalande, A., Zotti, C., Cervenansky, F., Yang, X., Heng, P.A., Cetin, I., Lekadir, K., Camara, O., Ballester, M.A.G., et al., 2018. Deep learning techniques for automatic mri cardiac multi-structures segmentation and diagnosis: Is the problem solved? *IEEE transactions on medical imaging* 37, 2514–2525.

- Chen, X., Yuan, Y., Zeng, G., Wang, J., 2021. Semi-supervised semantic segmentation with cross pseudo supervision, in: Proceedings of the IEEE/CVF Conference on Computer Vision and Pattern Recognition, pp. 2613–2622.
- Clark, K., Vendt, B., Smith, K., Freymann, J., Kirby, J., Koppel, P., Moore, S., Phillips, S., Maffitt, D., Pringle, M., et al., 2013. The cancer imaging archive (tcia): maintaining and operating a public information repository. *Journal of digital imaging* 26, 1045–1057.
- Esser, P., Sutter, E., Ommer, B., 2018. A variational u-net for conditional appearance and shape generation, in: Proceedings of the IEEE Conference on Computer Vision and Pattern Recognition, pp. 8857–8866.
- Gal, Y., Ghahramani, Z., 2016. Dropout as a bayesian approximation: Representing model uncertainty in deep learning, in: international conference on machine learning, PMLR. pp. 1050–1059.
- Jin, L., Lu, H., Wen, G., 2019. Fast uncertainty quantification of reservoir simulation with variational u-net. *arXiv preprint arXiv:1907.00718*.
- Jungo, A., Reyes, M., 2019. Assessing reliability and challenges of uncertainty estimations for medical image segmentation, in: International Conference on Medical Image Computing and Computer-Assisted Intervention, Springer. pp. 48–56.
- Kalluri, T., Varma, G., Chandraker, M., Jawahar, C., 2019. Universal semi-supervised semantic segmentation, in: Proceedings of the IEEE/CVF International Conference on Computer Vision, pp. 5259–5270.
- Kendall, A., Gal, Y., 2017. What uncertainties do we need in bayesian deep learning for computer vision? *arXiv preprint arXiv:1703.04977*.
- Laine, S., Aila, T., 2016. Temporal ensembling for semi-supervised learning. *arXiv preprint arXiv:1610.02242*.

- Lakshminarayanan, B., Pritzel, A., Blundell, C., 2016. Simple and scalable predictive uncertainty estimation using deep ensembles. arXiv preprint arXiv:1612.01474 .
- Lee, D.H., et al., 2013. Pseudo-label: The simple and efficient semi-supervised learning method for deep neural networks, in: Workshop on challenges in representation learning, ICML, p. 896.
- Li, S., Zhang, C., He, X., 2020. Shape-aware semi-supervised 3d semantic segmentation for medical images, in: International Conference on Medical Image Computing and Computer-Assisted Intervention, Springer. pp. 552–561.
- Luo, X., 2020. SSL4MIS. <https://github.com/HiLab-git/SSL4MIS>.
- Luo, X., Chen, J., Song, T., Wang, G., 2021a. Semi-supervised medical image segmentation through dual-task consistency, in: Proceedings of the AAAI Conference on Artificial Intelligence, pp. 8801–8809.
- Luo, X., Liao, W., Chen, J., Song, T., Chen, Y., Zhang, S., Chen, N., Wang, G., Zhang, S., 2021b. Efficient semi-supervised gross target volume of nasopharyngeal carcinoma segmentation via uncertainty rectified pyramid consistency, in: International Conference on Medical Image Computing and Computer-Assisted Intervention, Springer.
- Ma, J., Wei, Z., Zhang, Y., Wang, Y., Lv, R., Zhu, C., Gaoxiang, C., Liu, J., Peng, C., Wang, L., et al., 2020. How distance transform maps boost segmentation cnns: an empirical study, in: Medical Imaging with Deep Learning, PMLR. pp. 479–492.
- Masood, S., Sharif, M., Masood, A., Yasmin, M., Raza, M., 2015. A survey on medical image segmentation. Current Medical Imaging 11, 3–14.
- Milletari, F., Navab, N., Ahmadi, S.A., 2016. V-net: Fully convolutional neural networks for volumetric medical image segmentation, in: 2016 fourth international conference on 3D vision (3DV), IEEE. pp. 565–571.

- Mittal, S., Tatarchenko, M., Brox, T., 2019. Semi-supervised semantic segmentation with high-and low-level consistency. *IEEE transactions on pattern analysis and machine intelligence* .
- Miyato, T., Maeda, S.i., Koyama, M., Ishii, S., 2018. Virtual adversarial training: a regularization method for supervised and semi-supervised learning. *IEEE transactions on pattern analysis and machine intelligence* 41, 1979–1993.
- Ouali, Y., Hudelot, C., Tami, M., 2020. Semi-supervised semantic segmentation with cross-consistency training, in: *Proceedings of the IEEE/CVF Conference on Computer Vision and Pattern Recognition*, pp. 12674–12684.
- Pham, H., Dai, Z., Xie, Q., Le, Q.V., 2021. Meta pseudo labels, in: *Proceedings of the IEEE/CVF Conference on Computer Vision and Pattern Recognition*, pp. 11557–11568.
- Qiao, F., Peng, X., 2021. Uncertainty-guided model generalization to unseen domains, in: *Proceedings of the IEEE/CVF Conference on Computer Vision and Pattern Recognition*, pp. 6790–6800.
- Rizve, M.N., Duarte, K., Rawat, Y.S., Shah, M., 2021. In defense of pseudo-labeling: An uncertainty-aware pseudo-label selection framework for semi-supervised learning. *arXiv preprint arXiv:2101.06329* .
- Ronneberger, O., Fischer, P., Brox, T., 2015. U-net: Convolutional networks for biomedical image segmentation, in: *Proceedings of the International Conference on Medical Image Computing and Computer-Assisted Intervention (MICCAI)*, pp. 234–241. doi:[10.1007/978-3-662-54345-0_3](https://doi.org/10.1007/978-3-662-54345-0_3).
- Sohn, K., Berthelot, D., Li, C.L., Zhang, Z., Carlini, N., Cubuk, E.D., Kurakin, A., Zhang, H., Raffel, C., 2020. Fixmatch: Simplifying semi-supervised learning with consistency and confidence. *arXiv preprint arXiv:2001.07685* .

- Tarvainen, A., Valpola, H., 2017. Mean teachers are better role models: Weight-averaged consistency targets improve semi-supervised deep learning results. arXiv preprint arXiv:1703.01780 .
- Wang, Y., Huang, G., Song, S., Pan, X., Xia, Y., Wu, C., 2021. Regularizing deep networks with semantic data augmentation. *IEEE Transactions on Pattern Analysis and Machine Intelligence* .
- Wu, Y., Xu, M., Ge, Z., Cai, J., Zhang, L., 2021. Semi-supervised left atrium segmentation with mutual consistency training, in: *International Conference on Medical Image Computing and Computer-Assisted Intervention*, Springer.
- Xia, Y., Liu, F., Yang, D., Cai, J., Yu, L., Zhu, Z., Xu, D., Yuille, A., Roth, H., 2020. 3d semi-supervised learning with uncertainty-aware multi-view co-training, in: *Proceedings of the IEEE/CVF Winter Conference on Applications of Computer Vision*, pp. 3646–3655.
- Xie, Q., Dai, Z., Hovy, E., Luong, M.T., Le, Q.V., 2019. Unsupervised data augmentation for consistency training. arXiv preprint arXiv:1904.12848 .
- Xie, Y., Zhang, J., Liao, Z., Verjans, J., Shen, C., Xia, Y., 2020. Pairwise relation learning for semi-supervised gland segmentation, in: *International Conference on Medical Image Computing and Computer-Assisted Intervention*, Springer. pp. 417–427.
- Xiong, Z., Xia, Q., Hu, Z., Huang, N., Bian, C., Zheng, Y., Vesal, S., Ravikumar, N., Maier, A., Yang, X., et al., 2021. A global benchmark of algorithms for segmenting the left atrium from late gadolinium-enhanced cardiac magnetic resonance imaging. *Medical Image Analysis* 67, 101832.
- Yu, L., Wang, S., Li, X., Fu, C.W., Heng, P.A., 2019. Uncertainty-aware self-ensembling model for semi-supervised 3d left atrium segmentation, in: *International Conference on Medical Image Computing and Computer-Assisted Intervention*, Springer. pp. 605–613.

- Zhang, H., Cisse, M., Dauphin, Y.N., Lopez-Paz, D., 2017. mixup: Beyond empirical risk minimization. arXiv preprint arXiv:1710.09412 .
- Zhang, Y., Xiang, T., Hospedales, T.M., Lu, H., 2018. Deep mutual learning, in: Proceedings of the IEEE Conference on Computer Vision and Pattern Recognition, pp. 4320–4328.
- Zheng, Z., Yang, Y., 2021. Rectifying pseudo label learning via uncertainty estimation for domain adaptive semantic segmentation. International Journal of Computer Vision 129, 1106–1120.
- Zhou, Y., Li, Z., Bai, S., Wang, C., Chen, X., Han, M., Fishman, E., Yuille, A.L., 2019. Prior-aware neural network for partially-supervised multi-organ segmentation, in: Proceedings of the IEEE/CVF International Conference on Computer Vision, pp. 10672–10681.